

# Confocal Ellipsoidal Reflectors with Phased Array Vivaldi Antenna Source for Imaging Systems

Mohammad Hossein Koohi Ghamsari\*, Mahyar Mehri Pashaki<sup>†</sup>, Mehdi Ahmadi-Boroujeni<sup>‡</sup>,

\*Department of Electrical Engineering, Sharif University of Technology, Tehran, Iran, mohammad.koohi@sharif.edu

<sup>†</sup>Department of Electrical Engineering, Sharif University of Technology, Tehran, Iran, mahyar.mehri.p@gmail.com

<sup>‡</sup>Department of Electrical Engineering, Sharif University of Technology, Tehran, Iran, ahmadi@sharif.edu

**Abstract**—In this paper, an on-axis dual-reflector confocal ellipsoidal structure is presented for near-field imaging systems. In the proposed structure, the backscattered electromagnetic wave problem, known as the blockage effect, is reduced considerably using an elaborate design of the sub-reflector and precise alignment of the reflectors. The proposed geometry is analyzed, followed by a design example for the stand-off distance of 2 m. The blockage reduction characteristic is verified using ray-tracing simulation. Next, the scanning performance of the structure is investigated utilizing a Vivaldi phased array antenna as the source designed at the central frequency of 28 GHz. The full-wave simulations proved a field-of-view (FoV) of approximately 40 cm. Furthermore, tuning the proposed reflectors configuration stand-off distance is examined with a point source. The ray-tracing simulations showed that stand-off distance can be easily changed up to tens of centimeters with just a few centimeters of source point lateral displacement.

**Index Terms**—Reflector antenna, phased array antenna, Vivaldi antenna, blockage, imaging systems.

## I. INTRODUCTION

Nowadays, with the increasing expansion of telecommunication and imaging applications, designing suitable antenna structures is a crucial requirement [1]–[4]. The advantages of reflector antenna structures and reflective surfaces such as high gain and efficiency, wide-band operation, and a low sidelobe level (SLL), make these structures highly desirable for numerous applications in a wide range of electromagnetic spectrum, from microwave frequencies to millimeter-wave (mm-wave) and terahertz (THz) [5]–[11].

Reflector antenna systems have been designed for a wide range of applications. Reflector configurations are extensively utilized in telecommunications, facilitating long-distance signal transmission and reception with minimal interference [12]–[14]. In radio astronomy, reflector antennas enable the collection of faint signals from distant celestial bodies, enhancing our understanding of the universe [15], [16]. Additionally, reflector systems play a crucial role in radar technology, contributing to applications such as airport security and surveillance by providing precise target detection and tracking capabilities [17], [18]. Furthermore, reflectors are increasingly employed in satellite communication, where their ability to form multiple isolated beams allows for efficient frequency reuse and improved coverage [19].

In recent years, reflector antenna systems have played a crucial role in mm-wave and THz imaging systems by pro-

viding high gain, improved spatial resolution, the ability to effectively control beam patterns, and the ability to scan the focal plane easily, making them essential for high-resolution imaging systems [20]–[22]. Specifically, Gregorian-based reflector systems have attracted great attention for imaging in the near-field (Fresnel region), for scenarios such as focal plane imaging, due to their ability to control aberrations and thus provide acceptable scanning capabilities [23]. For example, a confocal Gregorian reflector system is designed for rapid scanning and refocusing of a THz beam for high-resolution stand-off imaging [24]. The proposed system achieves effective beam scanning over 0.5 m at a 25 m stand-off range, validated through numerical simulations while maintaining a minimal increase in beamwidth. The zooming and scanning capabilities of a Gregorian confocal dual reflector antenna, utilizing a planar feed array and active mechanical deformation to compensate for quadratic aberrations discussed [25]. A method to enhance THz imaging resolution in a dual reflector system is presented in [26], verified with a Gregorian system at 220 GHz, achieving better than 3 cm resolution over a 50 cm by 100 cm field-of-view (FoV) at 8 m, enabling active THz imaging of the human body.

However, there are still some drawbacks and challenges both in the design and performance of these reflector structures. First, many reflector configurations require large dimensions and complex designs, especially with multiple reflectors, which can complicate manufacturing and alignment processes. Second, quadratic aberrations may occur, necessitating active mechanical deformation to correct them, which adds to the complexity of the system. Third, reflector antennas can suffer from cross-polarization effects that degrade overall performance. Fourth, blockage can lead to reduced radiation efficiency, decreased signal-to-noise ratio (S/N), and diminished imaging systems detector sensitivity due to interference from return signals. Furthermore, the maximum scanning range can be restricted by blockage effects, impacting performance in many applications.

Various design techniques are proposed in the literature for improving the reflector antenna structures. Shaping and deforming reflectors using iterative approaches and asymmetric or off-axis techniques have been widely used for various optimization goals [27], [28]. However, each of these approaches has its own disadvantages. For instance, utilizing asymmetric or off-axis configurations for reducing the blockage increases

the overall system size and complexity in reflector manufacturing and alignment, as well as increasing the cross-polarization effects.

In this paper, a simple on-axis dual-reflector confocal ellipsoidal configuration with a Vivaldi phased array antenna as the feeding source is proposed for imaging in the Fresnel region. This structure is obtained by applying an elaborate modification to the traditional dual-reflector Gregorian structure. With these changes, the overall blockage effect is decreased considerably. Moreover, the scanning performance and tuning of the stand-off distance have been verified using full-wave and ray tracing simulations.

## II. CONFOCAL ELLIPSOIDAL STRUCTURE DESIGN

In this section, first, the general geometry of the proposed confocal ellipsoidal reflector system is presented and analyzed. Next, a design example is presented to verify the blockage reduction characteristic of our design by comparing it with a traditional Gregorian antenna structure.

### A. General Geometry

The general structure of the proposed symmetric dual-reflector configuration is depicted in Fig. 1. Similar to the standard Gregorian structure, a main reflector and sub-reflector are utilized with dimensions  $D_M$  and  $D_S$ , respectively. In comparison to reflector systems for telecommunication applications where the main reflector is a parabolic curve, here, the main reflector is a standard elliptical conic curve that is decentered vertically by  $D_B/2$ , leaving a hole in the middle of the geometry.  $P_2$  indicates the second focal point of the main reflector, located at the distance  $d_s$  in the focal plane. Also,  $F$  denotes the focal length of the main reflector.

The sub-reflector is also an elliptical conic curve that is simultaneously displaced and tilted counter-clockwise to share a common focus with the main reflector (point  $P_1$ ) and the source (point  $O$ ). The sub-reflector surface is produced from an ellipse with eccentricity  $e$  and interfocal distance  $2c$ . Symbols  $\theta_U$  and  $\theta_L$  show the upper and lower angles of the main reflector, respectively. Notation  $\theta_E$  represents the sub-reflector edge angle and  $\beta$  is the tilt angle between the symmetry axis and ellipse axis. Also,  $V_M$  and  $V_S$  denote the y-coordinates of the points on the main reflector and sub-reflector, respectively, corresponding to the principal ray of the geometry.

Based on Fig. 1, the main reflector and the sub-reflector curves can be generally described as

$$\overline{P_1M} = \frac{2F}{1 + \cos \theta_m} \quad (1)$$

$$\overline{OS} \mp \overline{SP_1} = \frac{2c}{e} \quad (2)$$

where  $\overline{P_1M}$  is the distance between the point  $P_1$  and point  $M$ ,  $\overline{OS}$  is the distance between the focal point  $O$  and the point  $S$  on the sub-reflector surface. Similarly,  $\overline{SP_1}$  is the distance

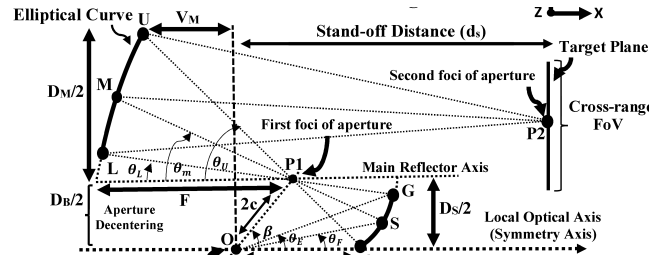


Fig. 1. Symmetric dual-reflector confocal ellipsoidal configuration. The modified displaced sub-reflector reflects the emanated rays from the source toward the main reflector. The elliptical main reflector, aperture, converges the divergent rays coming from the sub-reflector to the point  $P_2$ , the second foci of the aperture at the stand-off distance.

between point  $S$  and point  $P_1$ . Furthermore, from the basic trigonometric laws, it can be easily observed that

$$\tan \theta_U = \frac{-D_M}{2(V_S - V_M)} \quad (3)$$

The phase center of the electromagnetic source is located at point  $O$ . The basic geometrical optics and ray-tracing principles can be used to analyze the structure. First, the emanated divergent rays of the source incident on the exterior surface of the modified sub-reflector. Then, after reflection, the rays converge to point  $P_1$ , the first foci of the main reflector elliptical curve, and again diverge to the interior surface of the main reflector. Finally, the elliptical main reflector focuses the rays reflected from the sub-reflector at the Fresnel region at point  $P_2$ , the second focal point of the main reflector. Moreover, the field-of-view (FoV) can be defined as the maximum range of scanning the focus point within an acceptable range of aberrations and before the rays become increasingly divergent.

### B. Design Example

A design example is presented in this section to illustrate the ray's paths and blockage behavior of the structure. The design specifications are reported in Table I. According to this Table, the stand-off distance, where rays are focused, is considered 200 cm, and a FoV of approximately 40 cm is expected. Also, a standard Gregorian structure with the same specification is designed to compare the results.

The ray-tracing module of the COMSOL Multiphysics is adopted to perform the simulations. The obtained results are shown in Fig. 2. In this figure, the rays are colored based on the optical path length (OPL). It can be noticed that while no rays are blocked in the structure of Fig. 2 (a), a significant number of rays are blocked in the Gregorian structure of Fig. 2 (b), which proves the improved blockage performance of the proposed structure.

TABLE I  
DESIGN PARAMETERS OF THE CONFOCAL ELLIPSOIDAL STRUCTURE

$D_M$	$D_S$	$D_B$	$d_s$	FoV
80 cm	35 cm	16 cm	200 cm	40 cm

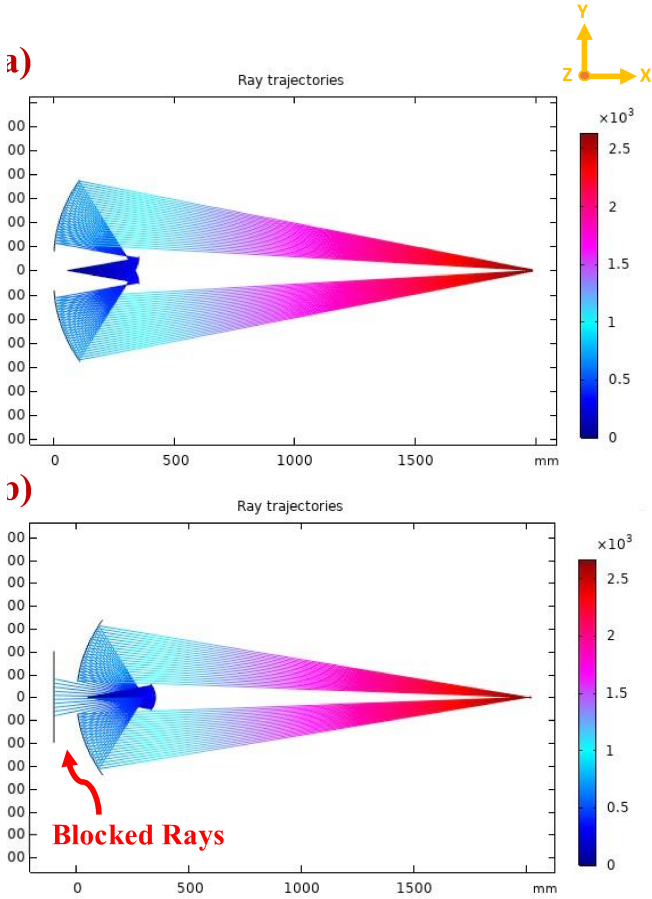


Fig. 2. Comparing the ray-tracing simulation results of the proposed structure and standard Gregorian. (a) Simulated rays' performance of the proposed dual-reflector confocal ellipsoidal structure. (b) Simulated rays' performance of the standard Gregorian structure. The color bar in both insets shows the optical path length (OPL) of the rays and the structure source point (O) is considered as the reference for the OPL calculations.

### III. EVALUATING IMAGING PERFORMANCE

The scanning performance and the tuning of the stand-off focusing distance, which are two critical abilities of an optical setup for imaging applications, are investigated in this section.

#### A. Scanning Performance

In this section, the capability of the proposed structure to scan in the near-field is examined. First, it is useful to have an intuition of the electric field (E-field) intensity distribution in the Fresnel region and also verify the focusing ability of the structure in a full-wave simulation. Therefore, the Electromagnetic Waves module of the COMSOL Multiphysics is utilized. As shown in Fig. 3, a point source is defined at point O of Fig. 1 at the frequency of 30 GHz. On the right side of this figure, the E-field intensity is maximized in a linear region, or E-field caustic. This is where the object can be located or displaced in an imaging scenario. The FoV can be defined as the maximum range of scanning the focus point within an acceptable value for the half-power-beamwidth (HPBW). To investigate the scanning performance

freq(1)=30 GHz Surface: ewfd.normE (V/m)

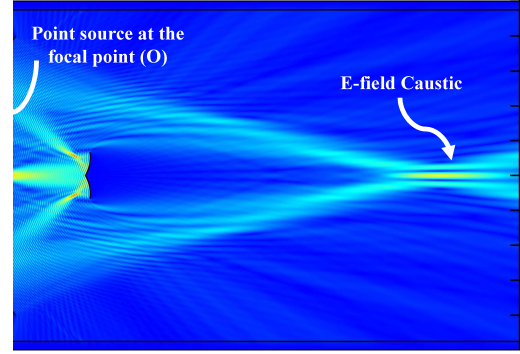


Fig. 3. Full-wave simulation of the dual-reflector confocal ellipsoidal Fresnel region.

of the proposed reflector configuration and calculate the FoV in a more practical approach, a phased array Vivaldi antenna is designed as the source of the structure for the central frequency of 28 GHz and beam steering capability from -30 to +30 degrees. The unit cell of this antenna is depicted in Fig. 4 (a) and the geometrical specifications are listed in Table II. The reflection coefficient of the unit cell is simulated using CST Studio Suite and is illustrated in Fig. 4 (b), displaying a 10-dB bandwidth ranging from 26 to 30 GHz. The overall structure of the antenna consisting of a 4x4 array of the proposed unit cells is also shown in Fig. 4 (c).

Using this Vivaldi phased array antenna in the dual-reflector structure as the source, the scanning performance of the structure is obtained as shown in Table III. Based on this table, by changing the phased array antenna beam angle by up to 30 degrees, the stand-off focusing point is scanned to about 19.7 cm, giving an approximate 40 cm desired FoV of Table I.

TABLE II  
GEOMETRICAL PARAMETERS OF THE VIVALDI ANTENNA UNIT CELL.

Parameter	Value (mm)	Parameter	Value (mm)
d	4.46	$L_s$	7.6
h	2	$L_1$	2.66
t	2.28	$L_2$	1
w	5.7	$L_3$	2
$w_a$	4.75	$L_4$	1.15
$w_t$	0.45	$L_5$	2
L	14.25	$L_6$	2

TABLE III  
SCANNING PERFORMANCE OF THE REFLECTOR STRUCTURE.

Phased array scanning (°)	±5	±10	±15	±20	±25	±30
Stand-off distance scanning (cm)	±3.5	±7.6	±10.3	±14.9	±18.6	±19.7

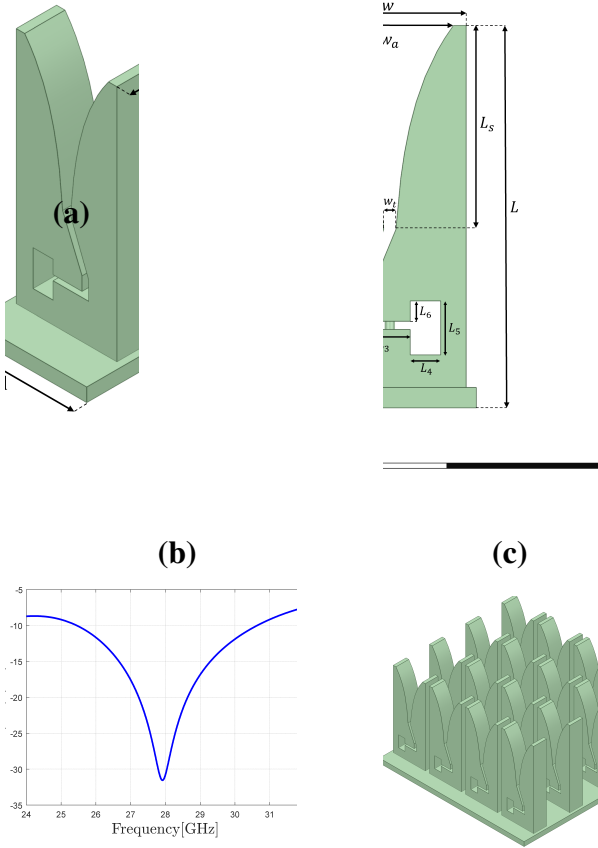


Fig. 4. Phased array Vivaldi antenna. (a) The proposed unit cell of the Vivaldi antenna. (b) Simulated reflection coefficient of the Vivaldi antenna unit cell. (c) Overall antenna array structure is composed of a 4×4 array of unit cells.

### B. Tuning Stand-off Distance

The focusing distance of the rays is an important specification for any imaging system. However, it is necessary for many applications to change this distance based on the imaging setup. Therefore, the dynamic tuning ability of the focusing distance, technically known as refocusing, is considered a critical advantage. In the proposed reflector system, the stand-off focusing distance is the second focal point of the main elliptical reflector. The equations governing the focal points of the main reflector are

$$\begin{aligned} d_1 &= \frac{r}{p} \left(1 - \sqrt{1-p}\right) \\ d_2 &= \frac{r}{p} \left(1 + \sqrt{1-p}\right) \end{aligned} \quad (4)$$

where  $d_1$  and  $d_2$  are the first and second focal lengths of the main reflector, respectively, and the relation  $d_2 = d_1 + 2c$  is always satisfied. Also, parameters  $r$  and  $p$  in these relations are the radius and the conic constant of the main reflector elliptical curve, respectively. Based on these relations and Fig. 5, the stand-off distance of the proposed structure can be easily tuned by the lateral displacement of the source point. To be more specific, by changing the feeding point about  $\Delta_{fx}$ , the stand-

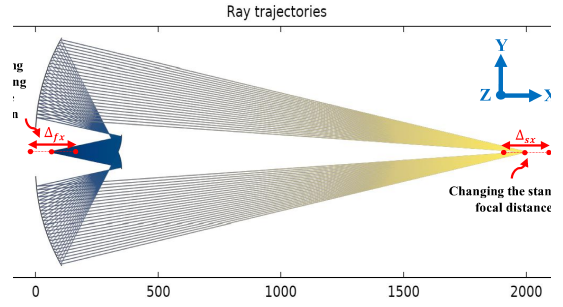


Fig. 5. Refocusing performance of the proposed structure by displacing the feeding source position laterally.

TABLE IV  
STAND-OFF DISTANCE TUNING USING FEED DISPLACEMENT AND MAGNIFICATION FACTOR.

$\Delta_{fx}$ [cm]	-2.5	-1.5	-0.5	3.5	1.5	0.5
$\Delta_{sx}$ [cm] ( $M_s = 6.5$ )	62	28	10	-48	-27	-13
$\Delta_{sx}$ [cm] ( $M_s = 2.5$ )	108	66	27	-99	-69	-25
$\Delta_{sx}$ [cm] ( $M_s = 11$ )	33	22	12	-26	-12	-6

off focusing point will also change about  $\Delta_{sx}$ . Some examples of these changes are listed in Table IV. In this table,  $M_s$  is the reflector system magnification factor and is defined as the ratio of the main reflector's first focal length to the sub-reflector's first focal length.

Based on Table IV, the stand-off distance has an inverse relation with the magnification factor. For example, by decreasing the magnification factor from 6.5 to 2.5,  $\Delta_{sx}$  is increased from 62 cm to 108 cm for  $\Delta_{fx} = -2.5$  cm. Furthermore, this table shows that by displacing the source point just a few centimeters, the stand-off focusing point can be tuned a few tens of centimeters. Additionally, these values are strongly dependent on the magnification factor of the reflector structure.

## IV. CONCLUSION

In this paper, a confocal ellipsoidal reflector system for near-field imaging applications is proposed. By effectively reducing the blockage effect through meticulous design and alignment of the reflectors, this configuration enhances the overall scanning performance and flexibility in tuning the focusing distance. Utilizing a Vivaldi phased array antenna and performing full-wave simulations, the capability of the presented structure to achieve a FoV of approximately 40 cm is demonstrated. The ray tracing simulation results presented dynamic adjustments in stand-off distance with minimal lateral displacement of the source point. Moreover, considering the reflector antenna frequency independence, the proposed structure can be effectively used in a wide range of the electromagnetic spectrum, from microwave and mm-wave imaging systems to THz imaging systems, with easily tunable properties for each imaging scenario.

## REFERENCES

- [1] C. A. Balanis, "The evolution of antenna technology: Reflectors and microstrips," *IEEE Antennas and Propagation Magazine*, 2024.

- [2] X. Shi, J. D. Peng, K. Huang, and L. H. Ye, "Broadband dual-polarized folded dipole antenna with simple feed structure," *Microwave and Optical Technology Letters*, vol. 65, no. 6, pp. 1735–1740, 2023.
- [3] W. Jiang, S. Liao, P. Liu, Q. Xue, and W. Che, "Millimeter-wave wideband $\pm 45^\circ$  dual-polarized wide-angle scanning phased array antenna," *IEEE Antennas and Wireless Propagation Letters*, 2024.
- [4] C. A. Balanis, *Antenna theory: analysis and design*. John Wiley & sons, 2016.
- [5] A. K. Baghel, V. U. Oliveira, P. Pinho, and N. B. Carvalho, "The novel method for deployable parabolic reflector based on uchiwa origami," in *2024 18th European Conference on Antennas and Propagation (EuCAP)*. IEEE, 2024, pp. 1–4.
- [6] D. Martinez-de Rioja, E. Martinez-de Rioja, Y. Rodriguez-Vaqueiro, A. Pino, C. Mosquera, J. A. Encinar, and G. Toso, "Multibeam compact dual reflectarray antenna for high-throughput satellites in ka-band," in *2024 18th European Conference on Antennas and Propagation (EuCAP)*. IEEE, 2024, pp. 1–4.
- [7] S. K. Vuyuru, R. Valkonen, D.-H. Kwon, and S. A. Tretyakov, "Efficient anomalous reflector design using array antenna scattering synthesis," *IEEE Antennas and Wireless Propagation Letters*, vol. 22, no. 7, pp. 1711–1715, 2023.
- [8] M. H. K. Ghamsari, E. Imanbeygi, and M. Ahmadi-Boroujeni, "Design of fresnel-region millimeter-wave metasurface beam shaper using deep learning," in *2024 32nd International Conference on Electrical Engineering (ICEE)*. IEEE, 2024, pp. 1–5.
- [9] M. Sano, R. Kuse, and T. Fukusako, "Reflection-phase calculation of circularly polarized folded reflectarray antennas with low profile, high efficiency, and arbitrary aperture distribution," *IEICE Communications Express*, 2024.
- [10] M. H. K. Ghamsari, M. Ahmadi-Boroujeni, and S. Babanejad, "A confocal ellipsoidal reflector system for millimeter-wave applications," in *2022 6th International Conference on Millimeter-Wave and Terahertz Technologies (MMWaTT)*. IEEE, 2022, pp. 1–4.
- [11] J. Sánchez-Pastor, M. Schüßler, R. Jakoby, and A. Jiménez-Sáez, "Double-layer frequency selective surface-based corner reflector for indoor self-localization systems in the w-band," in *2024 18th European Conference on Antennas and Propagation (EuCAP)*. IEEE, 2024, pp. 1–5.
- [12] S. Rao, L. Shafai, and S. K. Sharma, *Handbook of Reflector Antennas and Feed Systems Volume III: Applications of Reflectors*. Artech House, 2013.
- [13] D. T. Phan, J. Palosaari, D. Kong, T. Siponkoski, S. Myllymäki, M. E. Leinonen, A. Pärssinen, J. Juuti, and P. J. Soh, "Sub-thz spatially modulated beam splitting reflectors for potential ris implementations," in *2024 18th European Conference on Antennas and Propagation (EuCAP)*. IEEE, 2024, pp. 1–4.
- [14] J. Taillieu, D. González-Ovejero, R. Sauleau *et al.*, "Low-profile and broadband dual-linearly polarized offset dual-reflector antenna for w-band applications," *IEEE Transactions on Antennas and Propagation*, 2024.
- [15] J. W. Baars, *The paraboloidal reflector antenna in radio astronomy and communication*. Springer, 2007, vol. 348.
- [16] A. Soliman and S. Weinreb, "Optimization of small reflector antennas for radio astronomy," in *2016 United States National Committee of URSI National Radio Science Meeting (USNC-URSI NRSIM)*. IEEE, 2016, pp. 1–2.
- [17] A. G. Toshev, "Analysis, design and measurement of a low sidelobe level lightweight array antenna for surveillance radar applications," in *18-th International Conference on Microwaves, Radar and Wireless Communications*. IEEE, 2010, pp. 1–4.
- [18] J. Diao, "Poynting streamline for energy flow and aperture efficiency of reflector antennas: Application and analysis," *IEEE Antennas and Propagation Magazine*, 2024.
- [19] P. Robustillo, J. Rubio, R. Gómez-Alcalá, and J. Córcoles, "Spherical ports as a direct interface for full-interaction po/mom-to-fem: Application to lower-frequency satellite-remote-sensing reflector-based antennas," *IEEE Transactions on Antennas and Propagation*, 2024.
- [20] C. Rappaport and M. Geraghty, "A wideband reflector-based mm-wave/thz nearfield line scanner for rapidly sensing materials in envelopes," in *2024 18th European Conference on Antennas and Propagation (EuCAP)*. IEEE, 2024, pp. 1–3.
- [21] D. M. Sheen, D. L. McMakin, T. E. Hall, and R. H. Severtsen, "Active millimeter-wave standoff and portal imaging techniques for personnel screening," in *2009 IEEE Conference on Technologies for Homeland Security*. IEEE, 2009, pp. 440–447.
- [22] T. Wang, S. Luan, M. Yang, Y. Li, S. Xie, and Y. Yang, "A phase-controlled parabolic reflector for wideband microwave focal-plane imaging," *IEEE Antennas and Wireless Propagation Letters*, 2024.
- [23] M. H. K. Ghamsari, M. Ahmadi-boroujeni, and S. Babanejad, "Design and optimization of gregorian-based reflector systems for thz imaging system optics," in *2022 4th West Asian Symposium on Optical and Millimeter-wave Wireless Communications (WASOWC)*. IEEE, 2022, pp. 1–5.
- [24] N. Llombart, K. B. Cooper, R. J. Dengler, T. Bryllert, and P. H. Siegel, "Confocal ellipsoidal reflector system for a mechanically scanned active terahertz imager," *IEEE Transactions on Antennas and Propagation*, vol. 58, no. 6, pp. 1834–1841, 2010.
- [25] J. A. Martinez-Lorenzo, A. Garcia-Pino, B. Gonzalez-Valdes, and C. M. Rappaport, "Zooming and scanning gregorian confocal dual reflector antennas," *IEEE Transactions on antennas and propagation*, vol. 56, no. 9, pp. 2910–2919, 2008.
- [26] D. Zhou, L. Hou, Y. Yuan, Y. Zang, X. Tu, J. Chen, and P. Wu, "Bifocal dual reflector system for active terahertz imaging," *Applied optics*, vol. 57, no. 12, pp. 3224–3230, 2018.
- [27] M. Eichenberger, F. Giorgianni, N. Sauerwein, C. Vicario, and C. P. Hauri, "Deformable mirror for wavefront shaping of infrared radiation," *Optics Letters*, vol. 43, no. 9, pp. 2062–2065, 2018.
- [28] S. Kosulnikov, A. Diaz-Rubio, A. Osipov, and S. Tretyakov, "Experimental comparison of anomalous reflectors implemented with local and non-local design approaches," *IEEE Transactions on Antennas and Propagation*, 2024.